Gapped optical excitations from gapless phases: Imperfect nesting in unconventional density waves

Balázs Dóra* and András Virosztek
Department of Physics, Budapest University of Technology and Economics, H-1521 Budapest, Hungary

Kazumi Maki
Department of Physics and Astronomy, University of Southern California, Los Angeles, California 90089-0484, USA

Attila Virosztek
Department of Physics, Budapest University of Technology and Economics, H-1521 Budapest, Hungary and Research Institute for Solid State Physics and Optics, P.O. Box 49, H-1525 Budapest, Hungary
(Received 13 December 2004; revised manuscript received 27 January 2005; published 2 June 2005)

We consider the effect of imperfect nesting in quasi-one-dimensional unconventional density waves in the case in which the imperfect nesting and the gap depends on the same wave-vector component. The phase diagram is very similar to that in a conventional density wave. The density of states is highly asymmetric with respect to the Fermi energy. The optical conductivity at $T=0$ remains unchanged for small deviations from perfect nesting. For a higher imperfect nesting parameter, an optical gap opens, and a considerable amount of spectral weight is transferred to higher frequencies. This makes the optical response of our system very similar to that of a conventional density wave. Qualitatively similar results are expected in *d*-density waves.

DOI: 10.1103/PhysRevB.71.245101 PACS number(s): 71.45.Lr, 75.30.Fv, 72.15.Eb, 72.15.Nj

I. INTRODUCTION

The basic ingredient of the density wave (DW) formation is a band structure consisting of a pair of Fermi sheets, which can be nested to each other with a certain wave vector ($\mathbf{Q}$), giving rise to the density wave instability.[1] In real materials, however, this condition is not perfectly fulfilled: $\varepsilon(\mathbf{k})+\varepsilon(\mathbf{k}-\mathbf{Q})=2\eta(\mathbf{k})\neq 0$. In quasi-one-dimensional models studied during the early history of DW, one can choose it as $\eta(\mathbf{k})=\epsilon_0\cos(2bk_y)$, which shows the deviation from the one dimensionality.[2,3] In higher dimensional systems, different $\eta(\mathbf{k})$'s are deduced.[4] In conventional charge-density waves (CDWs) such as $NbSe_3$, the depression of the transition temperature under pressure is described in terms of the pressure dependence of imperfect nesting, and the large ratio of $2\Delta/T_c$ is also interpreted.[5–7] Similar to field-induced spin-density waves (FISDWs), many features are successfully described by this model.[2] The general consequence of ϵ_0 is the destruction of the density wave phase: imperfect nesting depresses the DW transition temperature and destroys completely the density wave when ϵ_0 becomes larger than a critical value. In addition, the imperfect nesting term gives rise to dip structures in the angle-dependent magnetoresistance in α-(BEDT-TTF)$_2$KHg(SCN)$_4$ (see Ref. 8) and Bechgaard salts (TMTSF)$_2$PF$_6$.[9] Imperfect nesting turned out to be crucial for the appearance of FISDW.[2] This motivates us to incorporate the effect of imperfect nesting in unconventional density wave (UDW) theory. UDW is a density wave whose gap function depends on the wave vector, and vanishes on certain points of the Fermi surface, allowing for low-energy excitations. The average of the gap function over the Fermi surface is zero, causing the lack of periodic modulation of the charge and spin density. Such systems have been studied and proposed over the years in a variety of systems.[10,11] These include heavy fermions like URu_2Si_2,[12–14] $CeCoIn_5$,[15] organic conductors as α-(BEDT-TTF)$_2$KHg(SCN)$_4$ (Ref. 16) and (TMTSF)$_2$PF$_6$,[9] high T_c superconductors.[17–19] Two different models are possible: two- (2D) or three-dimensional (3D) when the gap and the imperfect nesting depends on the same or different wave-vector component, respectively. Previously, we analyzed the properties of the 3D model,[20] and now we turn to the investigation of the 2D one.

The object of the present paper is to extend the analysis of Refs. 20 and 21 to the presence of imperfect nesting when the gap and the imperfect nesting depend on the same wave-vector component. We discuss the temperature dependence of the order parameter for different ϵ_0's. The phase boundary is almost the same as in a conventional DW. The chemical potential is shifted from its original value of the metallic state due to the presence of imperfect nesting. The temperature dependence of the order parameter, $\Delta(T,\epsilon_0)$ is anomalous; although it decreases monotonically with increasing temperature, it exhibits a sharp cusp at $\Delta(T,\epsilon_0)=2\epsilon_0$. In the density of states (DOS), the particle-hole symmetry is broken for the 2D model, leading to asymmetric density of states with respect to the Fermi energy. For high values of ϵ_0, the zero of the density of states at the Fermi energy disappears, and DOS becomes finite for all energies. Different optical responses are obtained depending on the electric field orientation and gap structure. The optical conductivity is not affected by the deterioration of perfect nesting in a wide parameter range. By further increasing ϵ_0, the divergent peak at 2Δ is divided into two new peaks. Moreover, a finite optical gap shows up at $T=0$ in spite of the finite density of states. Similar behavior was identified in a two-dimensional UDW (the so-called *d*-density wave[17]): deviations from perfect nesting induce a finite optical gap.[4] In clean systems, the weight of the Dirac delta peak at zero frequency is finite for

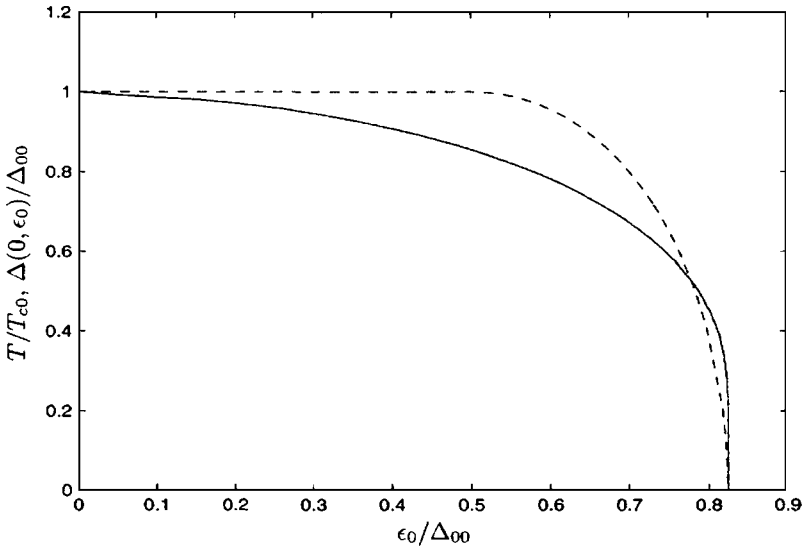

FIG. 1. The phase diagram (solid line) and the zero temperature order parameter (dashed line) are plotted in the presence of imperfect nesting.

all temperatures. We expect similar results in *d*-density waves as well.

II. PHASE DIAGRAM

To start with, we consider the Hamiltonian of interacting electrons:

$$H = \sum_{\mathbf{k},\sigma} \varepsilon(\mathbf{k}) a^{+}_{\mathbf{k},\sigma} a_{\mathbf{k},\sigma} + \frac{1}{2V} \sum_{\substack{\mathbf{k},\mathbf{k}',\mathbf{q} \\ \sigma,\sigma'}} \tilde{V}(\mathbf{k},\mathbf{k}',\mathbf{q}) a^{+}_{\mathbf{k}+\mathbf{q},\sigma} a_{\mathbf{k},\sigma} a^{+}_{\mathbf{k}'-\mathbf{q},\sigma'} a_{\mathbf{k}',\sigma'}, \quad (1)$$

where $a^{+}_{\mathbf{k},\sigma}$ and $a_{\mathbf{k},\sigma}$ are, respectively, the creation and annihilation operators of an electron of momentum $\mathbf{k}$ and spin σ. V is the volume of the sample. Our system is based on an orthogonal lattice, with lattice constants a, b, c toward directions x, y, z respectively. The system is anisotropic, the quasi-one-dimensional direction is the x axis. The kinetic-energy spectrum of the Hamiltonian is:

$$\varepsilon(\mathbf{k}) = -2t_a \cos(k_x a) - 2t_b \cos(k_y b) - 2t_c \cos(k_z c) - \mu, \quad (2)$$

which, in the vicinity of the Fermi surface, is well approximated by[5–7]

$$\varepsilon(\mathbf{k}) = \xi(\mathbf{k}) + \eta(\mathbf{k}), \quad (3)$$

where

$$\xi(\mathbf{k}) = v_F(|k_x| - k_F) - 2t_b \cos(k_y b) - 2t_c \cos(k_z c), \quad (4)$$

$$\eta(\mathbf{k}) = \epsilon_0 \cos(2bk_y), \quad (5)$$

$$\epsilon_0 = -\frac{t_b^2 \cos(ak_F)}{2t_a \sin^2(ak_F)}, \quad (6)$$

which is valid for $t_a \gg t_b \gg t_c$. In the second term of Eq. (1) we consider the interaction between on site and nearest neighbor electrons on the lattice; namely, on-site and nearest-neighbor direct Coulomb interaction, exchange, pair-hopping, and bond-charge terms. For a detailed description, see Refs. 21 and 22. This interaction is able to support a variety of low-temperature phases,[23] but we are only interested in unconventional DW (whose gap depends on the perpendicular momentum).[21,24] The latter can be either UCDW or USDW depending on the strength of the exchange and pair-hopping integrals. Within the mean-field approximation, the single-particle electron thermal Green's function using Nambu's notation is[25,26]

$$G_\sigma^{-1}(\mathbf{k}, i\omega_n) = i\omega_n - \eta(\mathbf{k}) - \xi(\mathbf{k})\rho_3 - \Delta_\sigma(\mathbf{k})\rho_1, \quad (7)$$

where ρ_i $(i=1,2,3)$ are the Pauli matrices acting on spinor space, and $\Delta_\sigma(\mathbf{k})$ is the UDW order parameter. In order to describe USDW, we assume Δ as an odd function of the spin $(\Delta_\sigma = -\Delta_{-\sigma})$. Assuming Δ_σ to be an even function of the spin, we would have UCDW. From now on, we will drop the spin indices since they are irrelevant for most of our discussion and most of our results apply to both unconventional charge and spin density waves. With this, the gap equation reads as

$$\Delta(\mathbf{l}) = \frac{1}{V} \sum_{\mathbf{k}} \overline{P(\mathbf{k},\mathbf{l})} \frac{\Delta(\mathbf{k})}{4E(\mathbf{K})} \times \left[\tanh\left(\frac{E(\mathbf{k}) + \eta(\mathbf{k})}{2T} \right) + \tanh\left(\frac{E(\mathbf{k}) - \eta(\mathbf{k})}{2T} \right) \right], \quad (8)$$

where $E(\mathbf{k}) = \sqrt{\xi(\mathbf{k})^2 + |\Delta(\mathbf{k})|^2}$, $\Delta(\mathbf{k}) = \Delta_\sigma(\mathbf{k})$ and the kernel of the integral equation is diagonal on the basis of the leading harmonics as[21]

$$\frac{P(\mathbf{k},\mathbf{l})}{V} = \frac{P_0}{N} + \frac{P_1}{N} \cos(k_y b)\cos(l_y b) + \frac{P_2}{N} \sin(k_y b)\sin(l_y b) + \frac{P_3}{N} \cos(k_z c)\cos(l_z c) + \frac{P_4}{N} \sin(k_z c)\sin(l_z c). \quad (9)$$

The P_i coefficients are linear combinations of the interaction

matrix elements. As a consequence of the general form of the kernel, the gap will be of the form

$$\Delta(\mathbf{l}) = \Delta_0 + \Delta_1 \cos(l_y b) + \Delta_2 \sin(l_y b) + \Delta_3 \cos(l_z c) + \Delta_4 \sin(l_z c). \tag{10}$$

From now on we assume that only one kind of gap among the five possible candidates, whose transition temperature is the highest, opens, and persists all the way down to zero temperature. For the stability of different phases, we refer the reader to Ref. 21. In quasi-one-dimensional systems, the gap function of UDW vanishes linearly on lines at the Fermi surface. Hence, the thermodynamics of UDW *in these systems* does not depend on the explicit wave-vector dependence of the gap; only transport properties are sensitive to the position of zeros of gap, and can distinguish between various gap structures.[21] It is worth noting, that in higher dimensional systems,[14] more complicated gap functions can be identified with line or point nodes, possessing distinct thermodynamical properties.

From Eq. (7), it is clear that the effect of imperfect nesting is incorporated in the theory by replacing the Matsubara frequency in the single-particle Green's function with $\omega_n + i[\epsilon_0 \cos(2bk_y) - \delta\mu]$,[27,28] where $\delta\mu$ is the change of the chemical potential due to the change in the spectrum. The order parameter[22] is assumed to depend on the wave-vector as $\Delta(\mathbf{k}) = \Delta \sin(bk_y)$ or $\Delta \cos(bk_y)$. Identical results are obtained for the k_z-dependent gap. The second-order phase boundary is given by $\epsilon_0 = \Delta_0(T_c)$, where $\Delta_0(T)$ is the temperature dependence of the gap in a perfectly nested conventional DW with T_{c0} transition temperature. T_{c0} is the transition temperature in the absence of imperfect nesting. This is almost the complete phase diagram. At high temperature when T becomes of order of ϵ_0, the deviation from perfect nesting becomes irrelevant, the best nesting vector is $\mathbf{Q} = (2k_F, \pi/b, \pi/c)$. In the conventional scenario, two DW phases can occur,[29] characterized by slightly different wave vectors and $\mathbf{Q}$ is replaced by a temperature-dependent wave vector, opening a narrow region above the critical nesting at low temperatures. For the present model, the possibility of ordering with different wave vector is there, although its examination is beyond the scope of the present discussion. The critical nesting is given by $\epsilon_0 = \sqrt{e}\Delta_{00}/2 \approx 0.82\Delta_{00}$, where Δ_{00} is the gap in a perfectly nested system at zero temperature. The order parameter remains unchanged for $\epsilon_0 < \Delta_{00}/2$, and vanishes sharply as ϵ_0 approaches its critical value. This together with the phase diagram is shown in Fig. 1. The most interesting consequence of imperfect nesting is that the chemical potential does not remain constant under the density wave formation. Its shift is given by

$$\delta\mu = \epsilon_0 \Theta[\Delta(T,\epsilon_0) - 2\epsilon_0] + \frac{\Delta(T,\epsilon_0)^2}{4\epsilon_0}\Theta[2\epsilon_0 - \Delta(T,\epsilon_0)], \tag{11}$$

where $\Theta(x)$ is the Heaviside function. This behavior can readily be seen from the density of states, where for any finite Δ, the total number of states below the Fermi energy is regained only by shifting the Fermi energy as given above. Note that this change belongs to a sinusoidal gap, while for a cosinusoidal gap the sign of the shift is reversed. The change in the spectrum in the presence of imperfect nesting is shown in Fig. 2, which is given by

$$E_{\pm}(\mathbf{k}) = \frac{\varepsilon(\mathbf{k}) + \varepsilon(\mathbf{k}-\mathbf{Q})}{2} \pm \sqrt{\left(\frac{\varepsilon(\mathbf{k}) - \varepsilon(\mathbf{k}-\mathbf{Q})}{2}\right)^2 + |\Delta(\mathbf{k})|^2}. \tag{12}$$

In the perfectly nested case, the low-energy part of the spectrum consists of Dirac cones with peaks at the Fermi energy.[21] For small ϵ_0, the spectrum is still crossed by the Fermi energy at the zeros of the gap. By increasing ϵ_0, a broad bump develops in the upper band, and crosses the Fermi energy. At this point, a large number of possible states becomes available, and the chemical potential starts decreasing to keep the total number of particles unchanged.

A direct consequence of this shift is a cusp in the temperature dependence of Δ at $\Delta = 2\epsilon_0$, since at this point the chemical potential changes. This feature is shown in Fig. 3, which is obtained from the numerical solution of the gap equation:

$$1 = TP\frac{N_0}{4}\sum_n \int_0^{2\pi} \frac{\sin^2(y)dy}{\sqrt{(\omega_n + i[\epsilon_0 \cos(2y) - \delta\mu])^2 + \Delta^2 \sin^2(y)}}, \tag{13}$$

where $P > 0$ is the interaction responsible for the UDW formation from Eq. (9), and N_0 is the density of states in the normal state at the Fermi energy per spin.

III. DENSITY OF STATES

The quasiparticle density of states is given by

$$g_{2D}(E) = N(x,a) = N_0 \int_0^{2\pi} \frac{dy}{2\pi} \mathrm{Re}\frac{|E + \delta\mu - \epsilon_0 \cos(2y)|}{\sqrt{[E + \delta\mu - \epsilon_0 \cos(2y)]^2 - \Delta^2 \sin^2(y)}}. \tag{14}$$

The energy variables are expressed in units of ϵ_0, i.e., $a = \Delta/\epsilon_0$ and $x = (E + \delta\mu)/\epsilon_0$, the energy is measured from the new Fermi energy. The density of states is obtained as

$$N(x,a) = N_0 \frac{1}{\pi\sqrt{pq}}\left[\left(x - 1 - \frac{2q}{p-q}\right)K\left(\frac{1}{2}\sqrt{\frac{1-(p-q)^2}{pq}}\right) + \frac{p+q}{p-q}\Pi\left(\frac{(p-q)^2}{-4pq}, \frac{1}{2}\sqrt{\frac{1-(p-q)^2}{pq}}\right)\right] \tag{15}$$

for $x > a^2/8 + 1$, where $p = \sqrt{(m-1)^2 + n^2}$, $q = \sqrt{m^2 + n^2}$, $m = [a^2 - 4(x-1)]/8$, $n = a\sqrt{-a^2 + 8(x-1)}/8$, and $K(z)$ and $\Pi(n,z)$ are the complete elliptic integrals of the first and

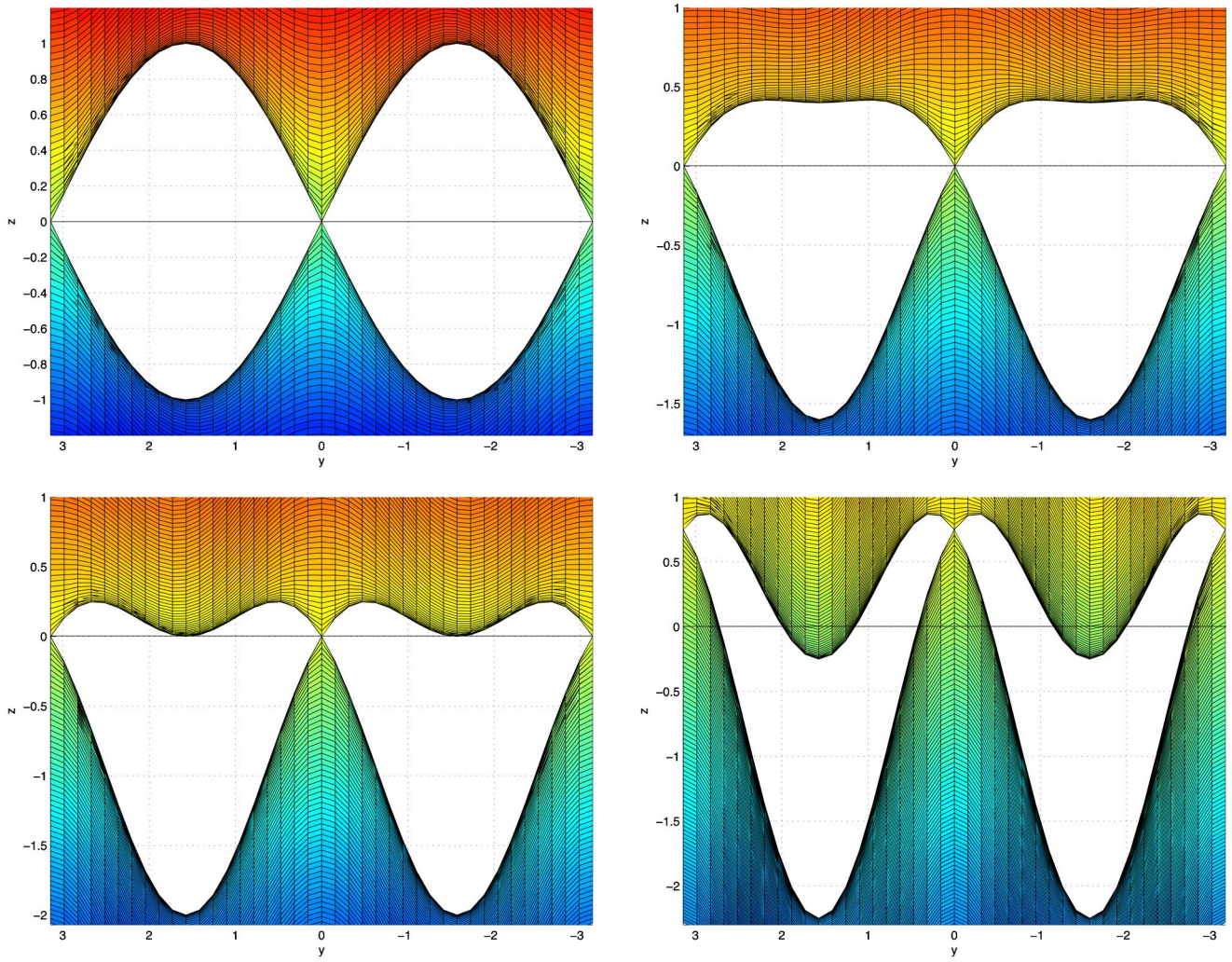

FIG. 2. The evolution of the quasiparticle spectrum is shown, viewed from the direction of the k_x axis, for $\Delta(\mathbf{k})=\Delta\sin(bk_y)$ in the presence of imperfect nesting for $\epsilon_0/\Delta=0$, 0.3, 0.5 and 1 from left to right, top to bottom. The horizontal line denotes the Fermi energy. The band structure is chosen as $\varepsilon(\mathbf{k})=-2t_a\cos(ak_x)-2t_b\cos(bk_y)+\varepsilon_0\cos(2bk_y)$ with parameters as $t_a/\Delta=2$, $t_b/\Delta=0.1$ at half-filling.

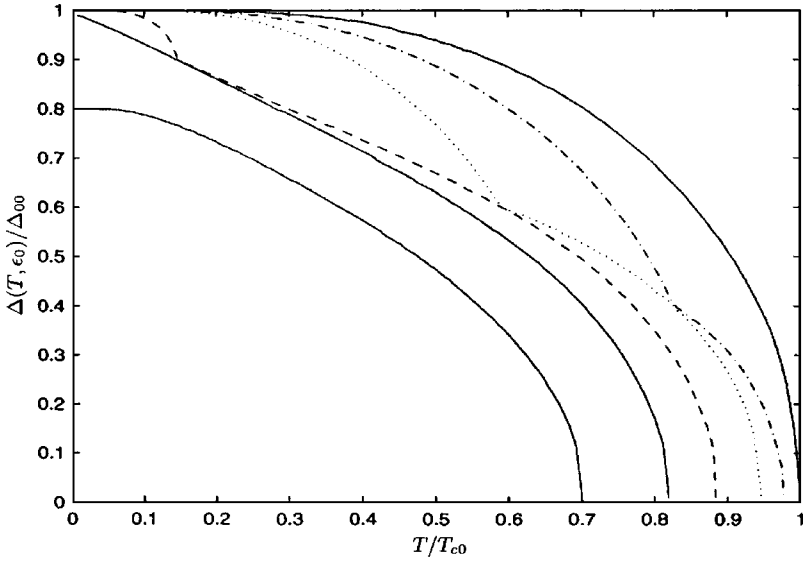

FIG. 3. The temperature dependence of the order parameter for the 2D model is shown for $\epsilon_0/\Delta_{00}=0$, 0.2, 0.3, 0.45, 0.55, and 0.7 from right to left. The cusp shows up only for $2\epsilon_0<\Delta_{00}$.

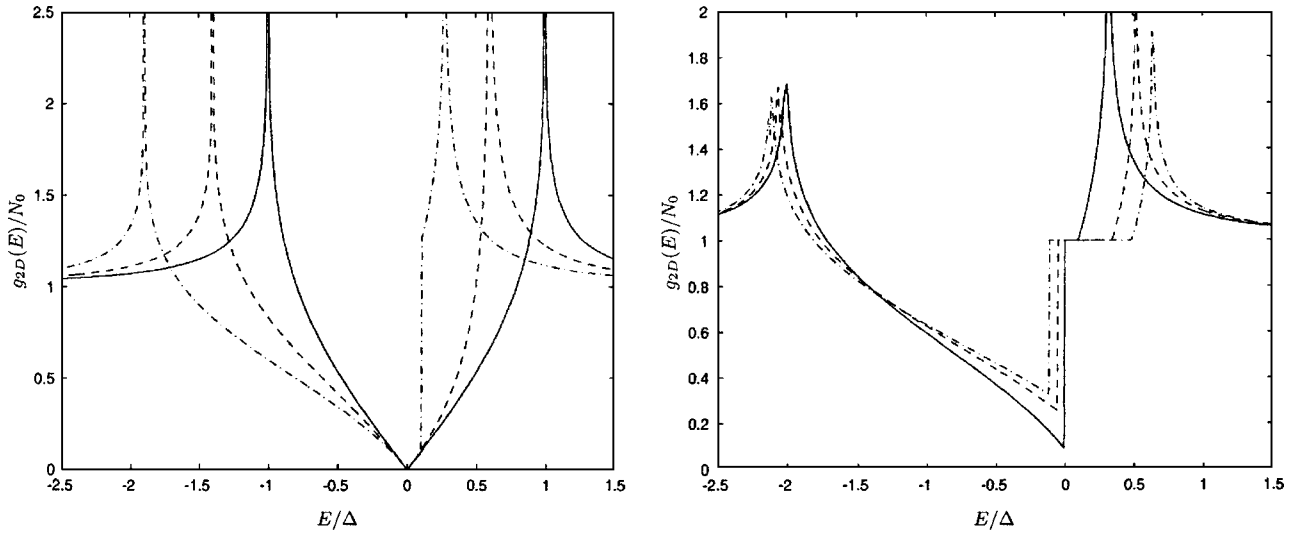

FIG. 4. The density of states as a function of energy is shown in the left panel for $\epsilon_0/\Delta=0$ (solid line), 0.2 (dashed line), and 0.45 (dashed-dotted line). In the right panel $\epsilon_0/\Delta=0.55$ (solid line), 0.7 (dashed line), and 0.8 (dashed-dotted line) are shown.

third kind, respectively.[30] In the remaining regions the DOS reads as

$$N(x,a) = N_0[\Theta(a-4)f_1(x,a) + \Theta(4-a)f_3(x,a)], \quad (a^2/8)+1 > x > a-1,$$

$$N(x,a) = N_0\,\mathrm{sgn}(x-1)f_2(x,a), \quad a-1 > x > -a-1,$$

$$N(x,a) = -N_0 f_3(x,a), \quad -a-1 > x, \tag{16}$$

where the following notations are used:

$$f_1(x,a) = \frac{1}{\pi\sqrt{(y_2-1)y_1}}\left[(x-1+2y_2)K\left(\sqrt{\frac{y_2-y_1}{(y_2-1)y_1}}\right) - 2y_2\Pi\left(\frac{1}{1-y_2}, \sqrt{\frac{y_2-y_1}{(y_2-1)y_1}}\right)\right], \tag{17}$$

$$f_2(x,a) = \frac{1}{\pi\sqrt{y_2-y_1}}\left[(x-1+2y_2)K\left(\sqrt{\frac{(y_2-1)y_1}{y_2-y_1}}\right) - 2y_2\Pi\left(\frac{y_1}{y_1-y_2}, \sqrt{\frac{(y_2-1)y_1}{y_2-y_1}}\right)\right], \tag{18}$$

$$f_3(x,a) = \frac{1}{\pi\sqrt{(1-y_1)y_2}}\left\{2(y_2-y_1)\Pi\left(\frac{y_2-1}{y_1-1}, \sqrt{\frac{(1-y_2)y_1}{(1-y_1)y_2}}\right) - 2\,\mathrm{sgn}(x-1)\Pi\left(\frac{y_1}{y_1-1}, \sqrt{\frac{(1-y_2)y_1}{(1-y_1)y_2}}\right) + [x-1+2y_1+\mathrm{sgn}(x-1)(x+1)] \times K\left(\sqrt{\frac{(1-y_2)y_1}{(1-y_1)y_2}}\right)\right\}, \tag{19}$$

and $y_1=[a^2-4(x-1)-a\sqrt{a^2-8(x-1)}]/8$, $y_2=[a^2-4(x-1)+a\sqrt{a^2-8(x-1)}]/8$.

The particle-hole symmetry is broken, which can be readily seen from the behavior of the peaks in the density of states, which slide from $\pm\Delta$ to $-\Delta-\epsilon_0-\delta\mu$ below the Fermi surface, while above it to $\Delta-\epsilon_0-\delta\mu$ for $4\epsilon_0<\Delta$ and to $\epsilon_0+\Delta^2/8\epsilon_0-\delta\mu$ otherwise. In addition, the zero in DOS is at the new Fermi energy for $\epsilon_0<\Delta/2$, and for larger ϵ_0 there exists no zero in the DOS. The density of states is plotted in Fig. 4. These statements correspond to $\Delta(\mathbf{k})=\Delta\sin(k_y b)$, while for a cosinusoidal gap $E\to -E$ change is needed in the density of states.

The residual density of states [i.e., $g_{2D}(E=0)$] is given by $N_0\Theta(2\epsilon_0-\Delta)$. Since on the Fermi surface the DOS vanishes in the same way for $\epsilon_0 \ll \Delta_{00}$ than in the perfectly nested case, the specific heat increases quadratically with temperature close to $T=0$ K in this region, while for large ϵ_0 it equals to the specific heat in the normal state.

IV. OPTICAL CONDUCTIVITY

In this section we investigate the quasiparticle contribution to the optical conductivity. For simplicity we neglect the effect of the quasiparticle damping due to impurity scattering for example. The quasiparticle part of the conductivity contains relevant information about the system in the perpendicular cases (y and z) when the effect of the collective contributions can be neglected. The regular part of the optical conductivity (without the Dirac delta) is given by

$$\mathrm{Re}\,\sigma^{reg}_{\alpha\beta}(\omega) = N_0\frac{\pi e^2}{\omega^2}\int_{-\pi}^{\pi}\frac{d(bk_y)}{2\pi}\int_{-\pi}^{\pi}\frac{d(ck_z)}{2\pi}\,\mathrm{Re}\,\frac{v_\alpha(\mathbf{k})v_\beta(\mathbf{k})\Delta^2(\mathbf{k})}{\sqrt{(\omega/2)^2-\Delta^2(\mathbf{k})}} \times\left[\tanh\left(\frac{|\omega|-2\eta}{4T}\right)+\tanh\left(\frac{|\omega|+2\eta}{4T}\right)\right], \tag{20}$$

where $v_\alpha(\mathbf{k})$ is the quasiparticle velocity in the α direction, $v_x(\mathbf{k})=v_F$, $v_y(\mathbf{k})=2bt_b\sin(bk_y)$, $v_z(\mathbf{k})=2ct_c\sin(ck_z)$, and $\eta=\epsilon_0\cos(2bk_y)-\delta\mu$. The wave-vector dependence of velocity

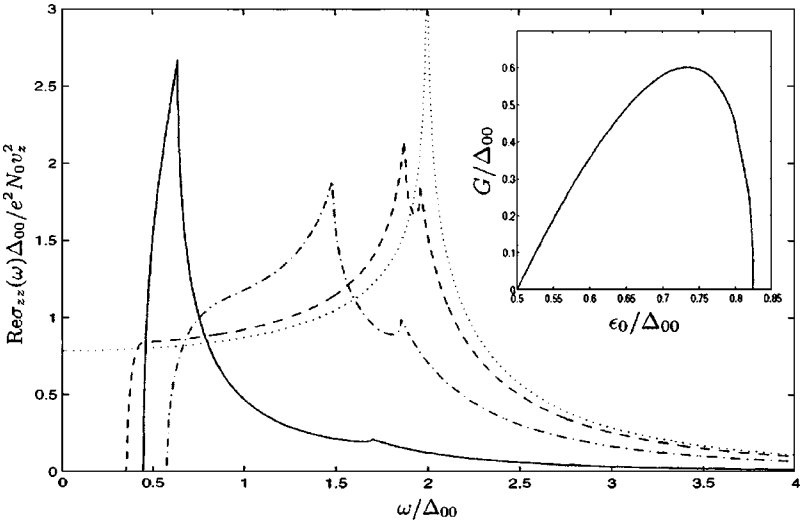

FIG. 5. The real part of the complex conductivity for the 2D model in the z direction is shown for $\epsilon_0/\Delta_{00}=0-0.5$ (dotted line), 0.6 (dashed line), 0.7 (dashed-dotted line), and 0.8 (solid line). Note that the same curves belong to $\sigma_{xx}(\omega)$ by changing v_z to v_F. The inset shows the ϵ_0 dependence of the optical gap. The same optical gap opens for other electric field orientations as well.

vertices distinguishes between the gaps with different wave-vector dependence, as we shall see below. From now on we restrict our investigation to the $T=0$ K case. The optical conductivity remains the same as in the perfectly nested case for $2\epsilon_0<\Delta(0,\epsilon_0)=\Delta_{00}$. For higher ϵ_0, the optical conductivity is zero for $\omega<G$, $G=\Delta(\sqrt{8-a^2}-a)/2$, similar to the effect of magnetic field where the $\omega<2\mu_B H$ part of the conductivity is chopped.[31] In other words, a clean optical gap develops for all electric field orientations. This can readily be observed in Fig. 2: when the upper band crosses the Fermi energy, the chemical potential moves below the zeros of the gap, suppressing the low-energy excitations, since only $\mathbf{q}=\mathbf{0}$ transitions are allowed for. Parallel to this the peak at 2Δ splits into two new peaks at $\Delta(\sqrt{8-a^2}+a)/2$ and at $\Delta(a/2+2/a)$. For $\omega>2\epsilon_0(1+a^2/4)$ the optical conductivity remains unchanged compared to Ref. 21. The only change in the remaining region can be expressed by redefining the I functions:[21]

$$I(\alpha,\beta,g)=\frac{\omega^2 g}{4\Delta^2}[F(g\sqrt{\beta},x)-F(g\sqrt{\alpha},x)-E(g\sqrt{\beta},x)+E(g\sqrt{\alpha},x)], \tag{21}$$

$$I_{\sin}(\alpha,\beta,g)=\frac{\omega}{12\Delta}\left\{\sqrt{\beta(1-\beta)\left[\left(\frac{\omega}{\Delta}\right)^2-4\beta^2\right]}-\sqrt{\alpha(1-\alpha)\left[\left(\frac{\omega}{\Delta}\right)^2-4\alpha^2\right]}+\left[\frac{\omega}{\Delta g}+\frac{1}{2}\left(\frac{\omega g}{\Delta}\right)^3\right][F(g\sqrt{\beta},x)-F(g\sqrt{\alpha},x)]-\left[\frac{2\omega g}{\Delta}+\frac{g}{2}\left(\frac{\omega}{\Delta}\right)^3\right][E(g\sqrt{\beta},x)+E(g\sqrt{\alpha},x)]\right\} \tag{22}$$

and $I_{\cos}(\alpha,\beta,g)=I(\alpha,\beta,g)-I_{\sin}(\alpha,\beta,g)$, where $F(z,k)$ and $E(z,k)$ are the incomplete elliptic integrals of the first and second kind, respectively, $x=2\Delta/\omega g^2$, and the arguments of the I functions are obtained as

$$\alpha=\max\left(0,\frac{1}{2}-\frac{a^2}{8}-\frac{a\omega}{4\Delta}\right), \tag{23}$$

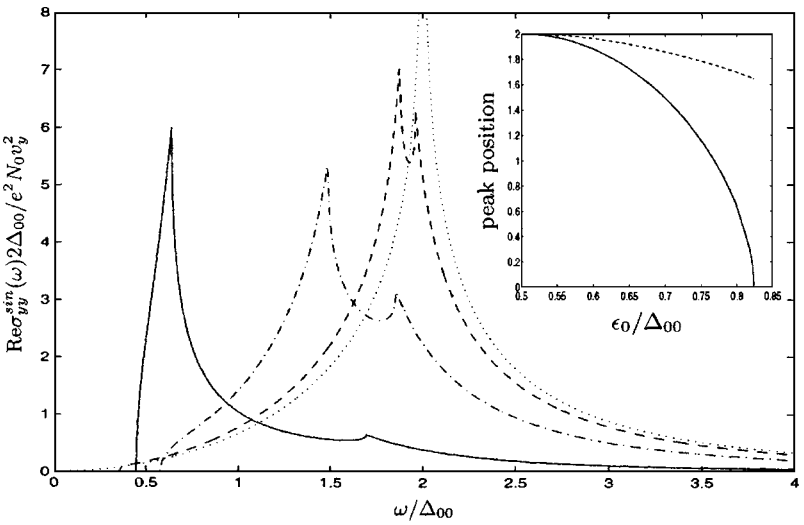

FIG. 6. The real part of the complex conductivity for the 2D model for a sinusoidal gap in the y direction is shown for $\epsilon_0/\Delta_{00}=0-0.5$ (dotted line), 0.6 (dashed line), 0.7 (dashed-dotted line), and 0.8 (solid line). The inset shows the ϵ_0 dependence of the peaks, which show up in all electric field orientations.

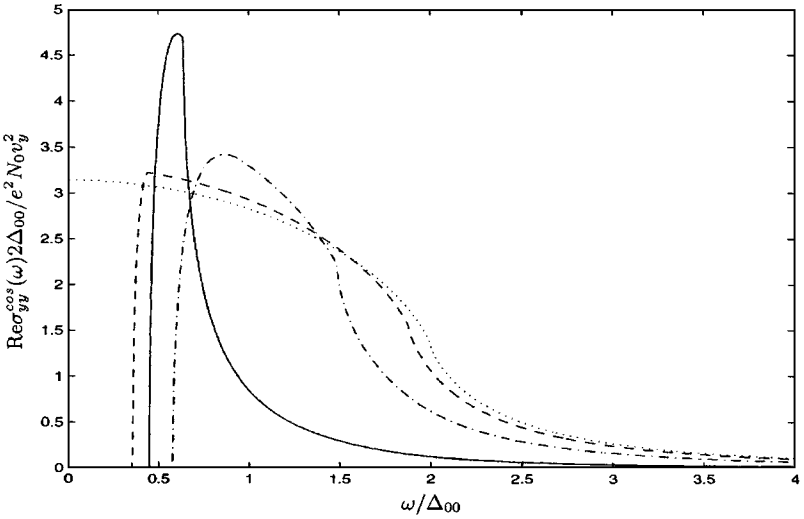

FIG. 7. The real part of the complex conductivity for the 2D model for a cosinusoidal gap in the y direction is shown for $\epsilon_0/\Delta_{00}=0$ (dotted line), 0.6 (dashed line), 0.7 (dashed-dotted line), and 0.8 (solid line).

$$\beta = \min\left[1, \frac{1}{2} - \frac{a^2}{8} + \frac{a\omega}{4\Delta}, \left(\frac{\omega}{2\Delta}\right)^2\right], \tag{24}$$

$$g = \max\left(1, \frac{2\Delta}{\omega}\right), \tag{25}$$

for $\omega > G$ and for $a < 2$. For $a > 2$, $\alpha = 0$, $\beta = 1$, and the I functions reduce to those in Ref. 21. Here, min and max give the largest and the smallest values of its arguments, respectively. With these notations the optical conductivity reads as

$$\mathrm{Re}\ \sigma_{yy}^{\sin,\cos}(\omega) = e^2 N_0 v_y^2 \frac{8\Delta(0,\epsilon_0)^2}{\omega^3} I_{\sin,\cos}(\alpha,\beta,g), \tag{26}$$

$$\mathrm{Re}\ \sigma_{zz}(\omega) = e^2 N_0 v_z^2 \frac{4\Delta(0,\epsilon_0)^2}{\omega^3} I(\alpha,\beta,g). \tag{27}$$

The optical conductivity in the three qualitatively different cases is shown in Figs. 5–7 with $v_x = v_F$, $v_y = \sqrt{2}bt_b$, and $v_z = \sqrt{2}ct_c$. In the x direction the quasiparticle part of the optical conductivity is the same as $\sigma_{zz}(\omega)$ if we replace v_z with v_F, although in the x direction it does not give the total conductivity since collective contributions change significantly the quasiparticle part, as was shown in Ref. 32. At first sight, the sum rule seems to be violated in all figures since a lot of optical weight is missing at small frequencies below the optical gap. However, the $\delta(\omega)$ part of the conductivity does not freeze out at $T \to 0$ in the presence of imperfect nesting, and its coefficient provides the missing area. As is well known, in the presence of impurity scattering, $\delta(\omega)$ changes to a Drude-like peak centered at $\omega = 0$. In Fig. 6, the low-energy excitations are suppressed because of the matching of the wave-vector dependence of the gap and velocity: low-energy excitations are only present in the system with zero weight. Similarly, the divergent peaks are missing from Fig. 7, since at the gap maximum the velocity of quasiparticles is zero. At finite temperature, the optical gap vanishes, but excitations below G are only possible with a probability of $\sim \exp\{-[\epsilon_0 - \Delta^2/(4\epsilon_0)]/T\}$.

V. CONCLUSION

We have studied theoretically the effect of imperfect nesting in unconventional density waves. Two qualitatively different cases are possible: the gap and imperfect nesting depend on the same (called the 2D model) or different wave-vector components (3D case).[20] Here we concentrated on the former. We explored the phase diagram which is identical to the one in a conventional density wave. The zero temperature gap function is not constant, contrary to the conventional case. The chemical potential changes compared to the normal state value. The density of states turned out to be asymmetric with respect to the Fermi energy due to the particle-hole symmetry breaking, but the logarithmically divergent peaks of the $\epsilon_0 = 0$ case remain present, but at different energies. For larger values of imperfect nesting $[2\epsilon_0 > \Delta(T, \epsilon_0)]$, the zero at the Fermi energy disappears, and the low-energy density of states regains its normal state form. Usually ϵ_0 is thought to vary with pressure providing the opportunity to check these results in a wide range of parameters. The optical gap of the model in the perpendicular optical conductivity can be observed experimentally at low temperatures. Moreover the splitting and lowering of the resonant peak at $\omega = 2\Delta$ (when the wave vector dependence of the gap and the velocity coincide) or its absence (for the other kind of gap)[20] could provide robust signatures of the microscopic nature of the low temperature phase.

ACKNOWLEDGMENTS

B.D. was supported by the Magyary Zoltán postdoctoral program of Foundation for Hungarian Higher Education and Research (AMFK). This work was supported by the Hungarian Scientific Research Fund under Grant Nos. OTKA TS040878, TS049881, T046269, and NDF45172.

*Electronic address: dora@kapica.phy.bme.hu

[1] G. Grüner, *Density Waves in Solids* (Addison-Wesley, Reading, 1994).
[2] T. Ishiguro, K. Yamaji, and G. Saito, *Organic Superconductors* (Springer, Berlin, 1998).
[3] G. Mihály, A. Virosztek, and G. Grüner, Phys. Rev. B **55**, R13456 (1997).
[4] D. N. Aristov and R. Zeyher, cond-mat/0406419 (unpublished).
[5] K. Yamaji, J. Phys. Soc. Jpn. **51**, 2787 (1982).
[6] K. Yamaji, J. Phys. Soc. Jpn. **52**, 1361 (1983).
[7] X. Huang and K. Maki, Phys. Rev. B **40**, 2575 (1989).
[8] K. Maki, B. Dóra, M. V. Kartsovnik, A. Virosztek, B. Korin-Hamzić, and M. Basletić, Phys. Rev. Lett. **90**, 256402 (2003).
[9] B. Dóra, K. Maki, A. Virosztek, and A. Ványolos, Europhys. Lett. **67**, 1024 (2004).
[10] A. H. Castro-Neto, Phys. Rev. Lett. **86**, 4382 (2001).
[11] A. A. Nersesyan and G. E. Vachnadze, J. Low Temp. Phys. **77**, 293 (1989).
[12] H. Ikeda and Y. Ohashi, Phys. Rev. Lett. **81**, 3723 (1998).
[13] A. Virosztek, K. Maki, and B. Dóra, Int. J. Mod. Phys. B **16**, 1667 (2002).
[14] Zs. Gulácsi and M. Gulácsi, Phys. Rev. B **36**, 699 (1987).
[15] B. Dóra, K. Maki, A. Virosztek, and A. Ványolos, Phys. Rev. B **71**, 172502 (2005); B. Dóra, K. Maki, A. Virosztek, and A. Ványolos, Phys. Status Solidi B **242**, 404 (2005).
[16] B. Dóra, K. Maki, and A. Virosztek, Mod. Phys. Lett. B **18**, 327 (2004).
[17] S. Chakravarty, R. B. Laughlin, D. K. Morr, and C. Nayak, Phys. Rev. B **63**, 094503 (2001).
[18] L. Benfatto, S. Caprara, and C. Di Castro, Eur. Phys. J. B **17**, 95 (2000).
[19] K. Maki, B. Dóra, A. Virosztek, and A. Ványolos, Curr. Appl. Phys. **4**, 603 (2004).
[20] B. Dóra, K. Maki, and A. Virosztek, Phys. Rev. B **66**, 165116 (2002).
[21] B. Dóra and A. Virosztek, Eur. Phys. J. B **22**, 167 (2001).
[22] B. Dóra, A. Virosztek, and K. Maki, Phys. Rev. B **66**, 115112 (2002).
[23] M. Ozaki, Int. J. Quantum Chem. **42**, 55 (1992).
[24] B. Dóra and A. Virosztek, J. Phys. IV **9**, Pr10-239 (1999).
[25] K. Maki, in *Superconductivity*, edited by R. D. Parks (Marcel Dekker, New York, 1969).
[26] G. Rickayzen, *Green's Functions and Condensed Matter* (Academic, London, 1980).
[27] X. Huang and K. Maki, Phys. Rev. B **42**, 6498 (1990).
[28] X. Huang and K. Maki, Phys. Rev. B **46**, 162 (1992).
[29] Y. Hasegawa and H. Fukuyama, J. Phys. Soc. Jpn. **55**, 3978 (1986).
[30] P. F. Byrd and M. D. Friedman, *Handbook of Elliptic Integrals for Engineers and Physicists* (Springer-Verlag, Berlin, 1954).
[31] B. Dóra, A. Virosztek, and K. Maki, Phys. Rev. B **65**, 155119 (2002).
[32] B. Dóra and A. Virosztek, Europhys. Lett. **61**, 396 (2003).